



Inflammatory Response and Defects on Myelin Integrity in the Olfactory System of K18hACE2 Mice Infected with SARS-CoV-2

 Eduardo Martin-Lopez,^{1,2} Bowen Brennan,^{1,2} Tianyang Mao,^{3,4,5} Natalie Spence,^{1,2} Sarah J. Meller,^{1,2,6} Kimberly Han,^{1,2} Nawal Yahiaoui,^{1,2} Chelsea Wang,^{1,2} Akiko Iwasaki,^{3,4,5} and  Charles A. Greer^{1,2,6}

¹Department of Neurosurgery, Yale University School of Medicine, New Haven, Connecticut 06520-8082, ²Department of Neuroscience, Yale University School of Medicine, New Haven, Connecticut 06520-8001, ³Department of Immunobiology, Yale University School of Medicine, The Anlyan Center, New Haven, Connecticut 06520-8043, ⁴Yale University School of Public Health, New Haven, Connecticut 06520-0834, ⁵Howard Hughes Medical Institute, Chevy Chase, Maryland 20815, and ⁶Interdepartmental Neuroscience Program, Yale University School of Medicine, New Haven, Connecticut 06520-8074

Abstract

Viruses, such as severe acute respiratory syndrome coronavirus 2 (SARS-CoV-2), use respiratory epithelial cells as an entry point for infection. Within the nasal cavity, the olfactory epithelium (OE) is particularly sensitive to infections which may lead to olfactory dysfunction. In patients suffering from coronavirus disease 2019, deficits in olfaction have been characterized as a distinctive symptom. Here, we used the K18hACE2 mice to study the spread of SARS-CoV-2 infection and inflammation in the olfactory system (OS) after 7 d of infection. In the OE, we found that SARS-CoV-2 selectively targeted the supporting/sustentacular cells (SCs) and macrophages from the lamina propria. In the brain, SARS-CoV-2 infected some microglial cells in the olfactory bulb (OB), and there was a widespread infection of projection neurons in the OB, piriform cortex (PC), and tubular striatum (TuS). Inflammation, indicated by both elevated numbers and morphologically activated IBA1⁺ cells (monocyte/macrophage lineages), was preferentially increased in the OE septum, while it was homogeneously distributed throughout the layers of the OB, PC, and TuS. Myelinated OS axonal tracts, the lateral olfactory tract, and the anterior commissure, exhibited decreased levels of 2',3'-cyclic-nucleotide 3'-phosphodiesterase, indicative of myelin defects. Collectively, our work supports the hypothesis that SARS-CoV-2 infected SC and macrophages in the OE and, centrally, microglia and subpopulations of OS neurons. The observed inflammation throughout the OS areas and central myelin defects may account for the long-lasting olfactory deficit.

Key words: inflammation; microglia; olfactory bulb; olfactory system; piriform cortex; SARS-CoV-2

Significance Statement

Damage to the olfactory system that can lead to loss of olfaction during coronavirus disease 2019 remains controversial. Using the K18hACE2 mouse infected with SARS-CoV-2, we show the infection of sustentacular cells and lamina propria macrophages in the olfactory epithelium but not the olfactory sensory neurons. In the brain, we found a widespread infection of projection neurons in the olfactory bulb (OB), piriform cortex, and tubular striatum, with microgliosis. Some SARS-CoV-2-infected microglia were observed in the OB. Alterations to the integrity of myelin in the olfactory tracts were evident. These data support the hypothesis of a nonolfactory entry pathway for SARS-CoV-2 into the brain, as well as the presence of impairments in neuronal conductivity in the olfactory tracts.

Received March 12, 2024; revised May 9, 2024; accepted May 24, 2024.

E.M.-L., T.M., B.B., N.S., S.J.M., K.H., N.Y., C.W., and C.A.G. authors declare no competing financial interests. A.I. co-founded RIGImmune, Xanadu Bio, and PanV and is a member of the Board of Directors of Roche Holding and Genentech.

Author contributions: E.M.-L., T.M., A.I., and C.A.G. designed research; E.M.-L., B.B., N.S., S.J.M., K.H., N.Y., and C.W. performed research; T.M. contributed unpublished reagents/analytic tools; E.M.-L., B.B., N.S., S.J.M., K.H., N.Y., C.W., A.I., and C.A.G. analyzed data; E.M.-L., T.M., A.I., and C.A.G. wrote the paper.

This work was supported by National Institutes of Health—National Institute on Deafness and Other Communication Disorders (NIH-NIDCD) 013791, NIH-NIDCD 016851, NIH-NIDCD 017989, and The Whitehall Foundation to C.A.G. and NIH R01AI157488, the Howard Hughes Medical Institute Collaborative COVID-19 Initiative, and the Howard Hughes Medical Institute Emerging Pathogens Initiative to A.I.; we express our appreciation to Christine Kaliszewski for her technical assistance and all members of the Greer and Iwasaki labs for their discussions.

Continued on next page.

Introduction

In 2019, SARS-CoV-2 (severe acute respiratory syndrome coronavirus 2) was identified as the pathological agent underlying coronavirus disease 2019 (COVID-19; Bergmann and Silverman, 2020; Huang et al., 2020). SARS-CoV-2 is characterized in part by the rapid infection of cells in the nasal cavity. The virus easily spreads into the lungs and other organs, causing severe inflammatory reactions and tissue damage (Brodin, 2021; Lamers and Haagmans, 2022; Merad et al., 2022; Priyal et al., 2023). The nasal cavity mucosa is covered by two epithelia: a ciliated, nonolfactory epithelium or respiratory epithelium (RE) that moistens and protects the airway from pathogens and the olfactory epithelium (OE) that contains the olfactory sensory neurons (OSNs; Fig. 1A; Harkema et al., 2006). In addition, OE includes sustentacular cells (SCs) or supporting cells that surround the OSNs. RE and SC express the angiotensin-converting enzyme 2 (ACE2) which is used for cell entry by SARS-CoV-2 and the protease TMPRSS2 which is important for cleavage and priming of the spike protein (Bilinska et al., 2020; Cooper et al., 2020; Fodoulian et al., 2020; Lee et al., 2020; Blume et al., 2021). Initially, the infection of SCs can impact the OSNs by limiting their nutrient support (Bilinska and Butowt, 2020; Khan et al., 2021, 2022) or indirectly by causing severe OE infiltration of immune cells, reduction of OSN neurogenesis, or disruption on the OSN expression of odorant receptors (Torabi et al., 2020; Finlay et al., 2022; Zazhytska et al., 2022). All direct and indirect damage to SCs can lead to a deficit in olfaction (Cooper et al., 2020; Tsukahara et al., 2023).

As COVID-19 progresses, a variety of neurological symptoms develop in up to 45% of patients (Priyal et al., 2023), suggesting that SARS-CoV-2 perturbs neuronal function. However, although the neuroinvasive potential of SARS-CoV-2 was proposed at the outset of the pandemic (L. Mao et al., 2020; Li et al., 2020; Moriguchi et al., 2020; Varatharaj et al., 2020), solid evidence to demonstrate neuronal infection in the human tissue remains in dispute. Several reports present compelling evidence of neuronal infection (Paniz-Mondolfi et al., 2020; Ramani et al., 2020; Burks et al., 2021; de Melo et al., 2021; Meinhardt et al., 2021; Song et al., 2021; Cappelletti et al., 2023; Yang et al., 2024), while others reported no direct infection of neurons (Brann et al., 2020; Pellegrini et al., 2020; Butowt et al., 2021, 2023; Khan et al., 2021; Finlay et al., 2022; Zazhytska et al., 2022; Luczo et al., 2024). Similarly, studies in laboratory animals report both the presence (Golden et al., 2020, 2022; Oladunni et al., 2020; Zheng et al., 2021; Beckman et al., 2022; Olivarria et al., 2022; Seehusen et al., 2022; Vidal et al., 2022; Yu et al., 2022; Villadiego et al., 2023; Shimizu et al., 2024) and absence (Bryche et al., 2020; Ye et al., 2021; Kishimoto-Urata et al., 2022; Verma et al., 2022) of neuronal infection. The possible role of brain infection of SARS-CoV-2 contributing to olfactory deficits in humans remains controversial (R. Choi et al., 2022). For example, Khan et al. (2021, 2022) found no evidence of infection in the CNS in a postmortem analysis of 68 individuals who died acutely diagnosed with SARS-CoV-2. However, the infection of the olfactory SC (cf. Khan et al., 2021) is widely accepted as an entry route that subsequently compromises odor receptor expression in sensory neurons (Frere et al., 2022; Zazhytska et al., 2022). Reports have also provided evidence of CNS infection in animals, including the olfactory system (OS) in hamsters (Frere et al., 2022), though the precise mechanisms providing access of SARS-CoV-2 into the brain remain under study. These include a hematopoietic route via infected macrophages or lymphocytes that extravasate the blood-brain barrier (BBB) or through breakdowns in the vasculature (Awogbindin et al., 2021; Kumari et al., 2021).

A definitive pathology that explains the diverse neurological symptoms, particularly in the OS, is still under debate. Some scientists argue that direct damage by SARS-CoV-2 to peripheral or central neurons, compromised myelin, and affected adult neurogenesis are still potential explanations for some of the symptoms of COVID-19 (Esposito et al., 2022, 2023; Fernandez-Castaneda et al., 2022; Lyoo et al., 2022; Stein et al., 2022; Ziuzia-Januszewska and Januszewski, 2022), although Monje and Iwasaki (2022) note that neuroinvasive infection in humans is rare.

To shed some light into the mechanisms of SARS-CoV-2 infections in olfactory pathways, we analyzed the spread of infection and neuroinflammation in the OS in K18hACE2 mice which can partially recapitulate the disease as seen in severely affected COVID-19 patients. Mice were infected with a previously determined dosage of virus that guaranteed the presence of pathology in brain tissues (Yinda et al., 2021; Dong et al.,

Correspondence should be addressed to Charles A. Greer at charles.greer@yale.edu or Akiko Iwasaki at akiko.iwasaki@yale.edu.

Copyright © 2024 Martin-Lopez et al. This is an open-access article distributed under the terms of the Creative Commons Attribution 4.0 International license, which permits unrestricted use, distribution and reproduction in any medium provided that the original work is properly attributed.

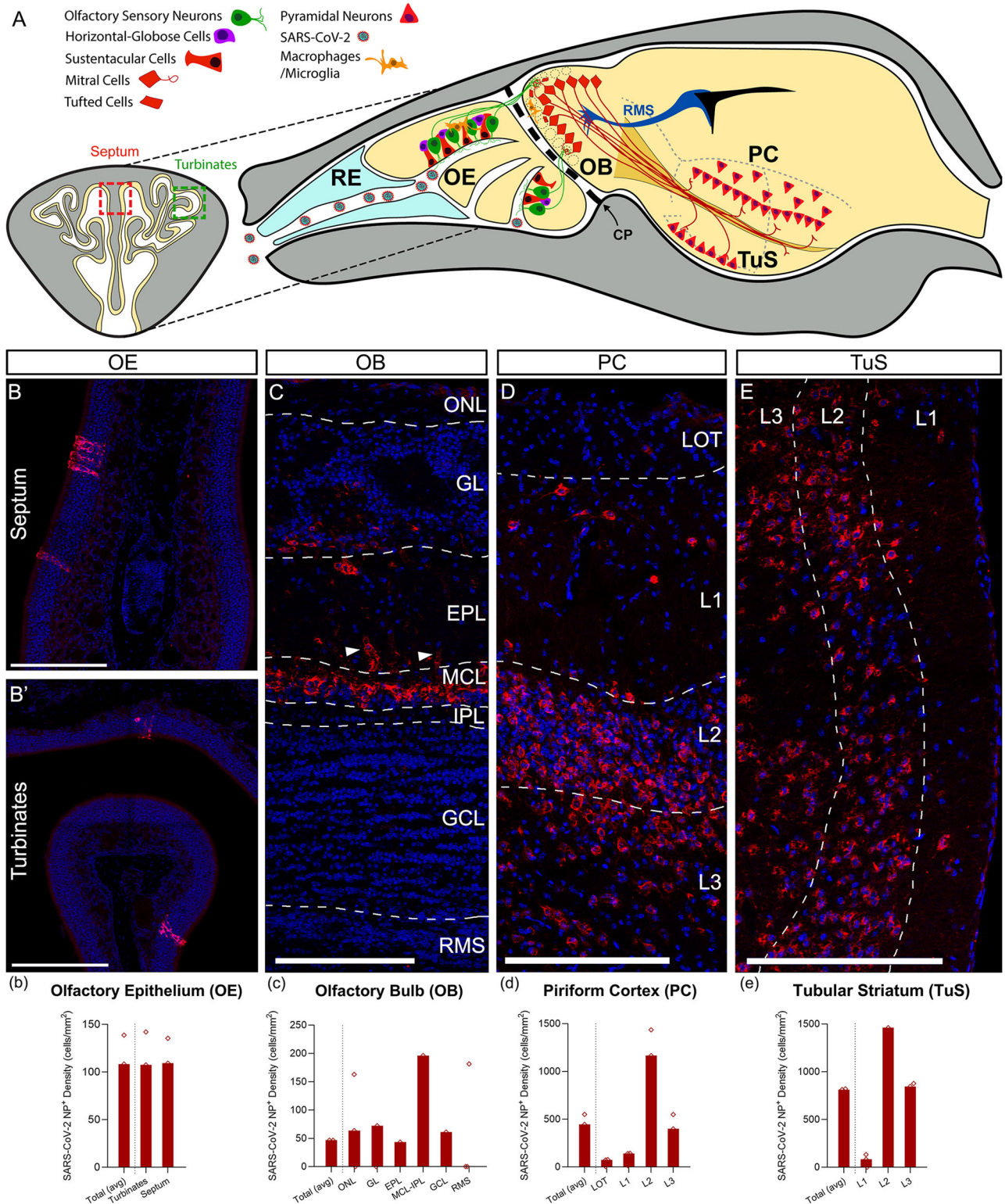


Figure 1. SARS-CoV-2 infection across the OS. **A**, Diagram illustrating a coronal (OE) and sagittal section (entire OS and brain) of K18hACE2 mice. Cells infected by SARS-CoV-2 are shown in red (neuronal) and orange (monocyte-macrophage lineages). **B–E**, Detection of SARS-CoV-2 nucleocapsid (red) with nuclei counterstained with DAPI (blue). **B–b**, SARS-CoV-2-infected cells appear as small clusters in the septum (**B**) and turbinates (**B'**). Quantification shows similar numbers of infected cells in both regions (**b**). **C, c**, SARS-CoV-2⁺ cells in the OB are predominantly accumulated around the MCL-IPL. Lower numbers are found in all other layers of the OB, including the most internal and external parts of the GL and EPL, respectively (**C**). Labeling of blood vessels is found in the EPL (**C**, arrowheads). **D, d**, SARS-CoV-2⁺ cells in PC showing extensive staining in the densely packed cell

2022; S. Choi et al., 2024). Using this experimental design, we addressed (1) the infection of the virus throughout the peripheral and central OS; (2) the characterization of infected cells; (3) the neuroinflammation caused by activated microglia; and (4) the effect on myelin along the olfactory myelinated tracts: the lateral olfactory tract (LOT) and the anterior commissure (AC).

Materials and Methods

Animals. All experiments were performed using 8-week-old male B6.Cg-Tg(K18-ACE2)2PrImn/J mice (common name, K18hACE2; McCray et al., 2007) obtained from Jackson Laboratory (jax.org/strain/034860). These mice express human angiotensin I-converting enzyme 2 (hACE2) under the regulation of the epithelial cell keratin-18 (K18) promoter. Animals were raised and maintained in a BSL3 facility at Yale University. All protocols were approved by Yale University Animal Care and Use Committee.

Generation of SARS-CoV-2 stocks. SARS-CoV-2 isolate hCoV-19/USA-WA1/2020 (NR-52281) was obtained from BEI Resources and subsequently amplified using VeroE6 cells overexpressing ACE2 and TMPRSS2 as previously described (T. Mao et al., 2022). Infectious viral titers were then determined by the plaque assay using Vero E6 cells overexpressing hACE2 and TMPRSS2.

SARS-CoV-2 intranasal inoculation. Mice were anesthetized using 30% v/v isoflurane diluted in propylene glycol and subsequently intranasally inoculated with 5×10^3 plaque-forming unit SARS-CoV-2 in 50 μ l (25 μ l per nostril) using a 200 μ l pipette.

Tissue processing and immunostaining. Seven days from infection, most animals lost 20% of body weight and became lethargic, meeting the euthanasia criteria. To obtain the OEs and brain tissues, animals were anaesthetized using a mixture of ketamine (50 mg/kg) and xylazine (5 mg/kg), injected intraperitoneally, and perfused first with 20 ml of PBS followed by 20 ml of ice-cooled 4% paraformaldehyde (PFA) in PBS. The heads were removed and fixed in 4% PFA overnight on a rotator. Then, entire brains were dissected from skulls and transferred to 30% sucrose in PBS for cryoprotection. OEs were first decalcified by immersing the entire nose containing the nasal cavity on 0.5 M EDTA for 1 month, then washed several times with PBS until the pH was neutralized, and finally transferred to a 30% sucrose in PBS for cryoprotection. Both OE and brains were embedded in Tissue-Tek optimal cutting temperature (OCT) compound (Thermo Fisher Scientific, catalog #4585) before being frozen for cryosectioning. Using a Reichert Frigocut cryostat (E-2800), we collected 25 μ m serial sections on Fisherbrand ColorFrost Plus slides (Thermo Fisher Scientific) at the coronal plane, then dried using a slide warmer at 55°C, and stored at -80°C until use.

For immunohistochemistry (IHC), sections were thawed in a slide warmer at 60°C for 20 min and then washed with PBS to remove the OCT compound. Next, slides were immersed into a 0.01 M citrate buffer (pH 6.0) at 65°C for 35 min, followed by a 5 min incubation in ice-cooled 0.01 M citrate buffer, pH 6.0, to perform an antigen unmasking. Slides were placed horizontally in a humid chamber, and sections were washed three times, 10 min each with PBS + 0.1% Triton X-100 (Millipore Sigma, catalog #x100; PBST) before blocking for 1 h at room temperature (RT), with a solution made of PBST supplemented with 5% normal donkey serum (SouthernBiotech, catalog #0030-01) and 0.01% of protease-free bovine serum albumin (Sigma-Aldrich, catalog #A3059). Primary antibodies were diluted in 10% diluted blocking solution (Table 1), and sections were incubated with them overnight at 4°C. Slides were washed three times with PBST for 10 min, and appropriate secondary antibodies (Table 1), supplemented with 1 μ g/ml of DAPI (Invitrogen, catalog #1306), were incubated for 2 h at RT. Finally, sections were washed three times for 10 min each with PBST, and slides were mounted with Mowiol 4-88 (Sigma-Aldrich, catalog #81381) prepared in 0.1 M Tris-glycerol.

Imaging, quantifications, and statistics. To analyze the morphology of microglial cells in response to the SARS-CoV-2 infection, we performed a fractal analysis similar to the methods reported before (Soltys et al., 2001; Meller et al., 2023). Individual microglia cells (IBA1⁺) were randomly selected in Layers 1 and 2 of the piriform cortex (PC) and imaged with a ZEISS LSM 900 confocal microscope using a 63 \times objective. Three images of an IBA1⁺ cells were selected per animal for 18 total images for analysis. Images from the Alexa Fluor 488 channel were preprocessed using ImageJ Macro to binarize the image and isolate ionized calcium-binding adapter molecule 1 (IBA1) stained pixels from the background. Using the paintbrush tool, adjacent cell processes and background noise were removed. The binary image was converted to an outline using the ImageJ outline tool. The FracLac ImageJ plugin was used to perform fractal analysis on the outline. Num G was set to 4, and the metrics, convex hull, and bounding circle options were checked. The fractal dimension (D_B), which

←
Layers 2 and 3 and in horizontal cells in Layer 1, located beneath the LOT (D). E, e, SARS-CoV-2⁺ cells in TuS accumulated mostly in the densely packed cell Layers 2 and 3. CP, cribriform plate; EPL, external plexiform layer; GCL, granule cell layer; GL, glomerular layer; IPL, internal plexiform layer; LOT, lateral olfactory tract; MCL, mitral cell layer; OB, olfactory bulb; OE, olfactory epithelium; ONL, olfactory nerve layer; PC, piriform cortex; RE, respiratory epithelium; RMS, rostral migratory stream (bulbar part); TuS, tubular striatum. Statistics in Table 2. Scale bars: 200 μ m.

Table 1. Primary and secondary antibodies

| Antigen | Primary Ab | Source (catalog #) | Dilution | Secondary Ab | Source | Dilution |
|----------------------------|-----------------------------|---|----------|---|--------------------------|----------|
| CNPase | Goat Poly. | Novus Biologicals (NBP3-05551) RRID: AB_3076521 | 1:1,000 | Donkey anti-goat IgG Alexa Fluor 647 | Thermo Fisher Scientific | 1:1,000 |
| Cytokeratin 8 | Rabbit clone EP1628Y | Abcam (ab53280) RRID: AB_869901 | 1:300 | Donkey anti-Rb IgG Alexa Fluor 488 | Thermo Fisher Scientific | 1:1,000 |
| CLEC7A (Dectin-1) | Rat IgG2a, κ | InvivoGen (mabg-mdect) RRID: AB_2753143 | 1:30 | Donkey anti-rat IgG Alexa Fluor 555 | Thermo Fisher Scientific | 1:1,000 |
| Ctip2 | Rat IgG2a | Abcam (ab18465) RRID: AB_2064130 | 1:500 | Donkey anti-rat IgG Alexa Fluor 488 and 647 | Thermo Fisher Scientific | 1:1,000 |
| IBA1 | Rabbit Poly. | FUJIFILM Wako Chemicals (016-20001) RRID: AB_839506 | 1:200 | Donkey anti-Rb IgG Alexa Fluor 488 | Thermo Fisher Scientific | 1:1,000 |
| OMP | Goat Poly. | FUJIFILM Wako Chemicals (019-22291) RRID: AB_664696 | 1:500 | Donkey anti-goat Alexa Fluor 647 | Thermo Fisher Scientific | 1:1,000 |
| Reelin recombinant | Rabbit clone EPR26278-30 | Abcam (ab312310) RRID: AB_3076463 | 1:100 | Donkey anti-Ms IgG Alexa Fluor 488 | Thermo Fisher Scientific | 1:1,000 |
| SARS-CoV-2 Nucleocapsid | Mouse IgG | Sino Biological (40143-MM05) RRID: AB_2827977 | 1:100 | Donkey anti-Ms IgG Alexa Fluor 555 | Thermo Fisher Scientific | 1:1,000 |
| Sox2 | Rat IgG2a, κ | Thermo Fisher Scientific (14-9811-82) RRID: AB_11219471 | 1:500 | Donkey anti-rat IgG Alexa Fluor 488 | Thermo Fisher Scientific | 1:1,000 |
| Tbr1 | Rabbit Poly. | Abcam (ab31940) RRID: AB_2200219 | 1:500 | Donkey anti-Rb IgG Alexa Fluor 488 | Thermo Fisher Scientific | 1:1,000 |

quantifies cell complexity, was recorded. Differences between control noninfected and SARS-CoV-2-infected groups were assessed using a Welch's unpaired *t* test in the GraphPad Prism 10.1.2 software. $P \leq 0.05$ was considered statistically significant (Table 2). Data is presented as mean \pm SEM.

To quantify the number of cells infected with SARS-CoV-2, we used the antibody that recognizes the nucleocapsid protein of the virus (SARS-CoV-2-NC⁺). To study inflammation, we used the staining for IBA1⁺ (microglial cells), as well as IBA⁺/Clec7A⁺, to determine the phagocytic-activated microglia. All images were acquired in a ZEISS LSM 800 confocal microscope using the 10 \times /20 \times objectives along the different OS areas: (1) the OE; (2) the olfactory bulb (OB); (3) the anterior PC; and (4) the tubular striatum (TuS), formerly the olfactory tubercle (Wesson, 2020). The OE was divided into two subsections, the septum and turbinates, and cells were quantified within the area from the edge of the epithelium to the lamina propria in randomly selected sections along the anterior to posterior axis. The OB was divided into its constituent layers, the olfactory nerve layer (ONL), glomerular layer (GL), external plexiform layer (EPL), mitral cell and internal plexiform layers (MCL-IPL) combined, granule cell layer (GCL), and the bulbar part of the rostral migratory stream (RMS), and quantified across the medial-lateral plane. The PC was divided into and quantified within its four layers: the LOT and Layers 1–3. The TuS was divided into and quantified within its three layers (1–3). The number of cells expressing the different markers were manually counted using ImageJ on 20 \times magnification confocal images. Cell counts were divided by their respective areas to calculate the average count per area. For each marker, images of the respective OS areas were captured across three consecutive sections separated by 250 μ m. Images were taken in a total of three mice ($N = 3$) per group (noninfected controls vs SARS-CoV-2). Raw data were adjusted to represent the number of cells per mm² before the statistical analysis. Statistical comparisons between the regions/layers for each olfactory area were made conducting a two-way ANOVA for SARS-CoV-2 quantifications and multiple unpaired *t* tests for IBA⁺ and IBA⁺/Clec7A⁺ using the GraphPad Prism 10.1.2 software. $P \leq 0.05$ was considered statistically significant (Table 2). Data is presented as mean \pm SEM.

The effect on myelin was studied in the main olfactory tracts: the AC and the LOT. Images were taken in the coronal plane with a ZEISS LSM 900 confocal microscope using a 20 \times objective. Two and three sections per animal were obtained for the AC and LOT, respectively. Myelin damage was measured by analyzing the 2',3'-cyclic-nucleotide 3'-phosphodiesterase (CNPase) labeling intensity, which is an indirect indicator of myelin integrity. Images were processed using ImageJ Macro to binarize the image and isolate CNPase stained pixels from the background. Using a fixed area within the AC and LOT, the intensity of all CNPase pixels was measured and averaged to obtain the average intensity of the stained pixels. Statistical comparisons were made running a multiple unpaired *t* test using the GraphPad Prism 10.1.2 software. $P \leq 0.05$ was considered statistically significant (Table 2). Data is presented as mean \pm SEM.

Table 2. Statistical analysis with significance

| Analysis/figure | Test | Statistical value | Pairwise comparisons | <i>p</i> value | | |
|--|--|---|--|-------------------------------------|-------------------|----------|
| Number of SARS-CoV-2 cells (Fig. 2) | Two-way ANOVA + Tukey's multiple-comparison test | Mean diff. -851.7 95.00% CI of diff. -1,601 to -102.5 | PC - LOT vs L1 | 0.0202 | | |
| | | Mean diff. -804.3 95.00% CI of diff. -1,554 to -55.13 | PC - L1 vs L2 | 0.0309 | | |
| | | Mean diff. -964.2 95.00% CI of diff. -1,920 to -8.442 | TuS - L1 vs L2 | 0.0476 | | |
| Fractal analysis (cell morphology; Fig. 3) | Welch's unpaired <i>t</i> test | <i>t</i> = 3.746, <i>df</i> = 12.58 | Control vs infected | 0.0026 | | |
| Macrophages counts in the OE (Fig. 4) | Multiple unpaired <i>t</i> tests | <i>t</i> = 2.917, <i>df</i> = 4.000 | IBA1 ⁺ in septum | 0.0434 | | |
| Microglia counts in the OB (Fig. 5) | Multiple unpaired <i>t</i> tests | <i>t</i> = 5.104, <i>df</i> = 4.000 | IBA1 ⁺ total (average) | 0.006963 | | |
| | | <i>t</i> = 3.147, <i>df</i> = 4.000 | IBA1 ⁺ /Clec7A ⁺ total (average) | 0.034601 | | |
| | | <i>t</i> = 3.992, <i>df</i> = 4.000 | IBA1 ⁺ in ONL | 0.016240 | | |
| | | <i>t</i> = 3.955, <i>df</i> = 4.000 | IBA1 ⁺ in GL | 0.016746 | | |
| | | <i>t</i> = 5.812, <i>df</i> = 4.000 | IBA1 ⁺ /Clec7A ⁺ in GL | 0.004362 | | |
| | | <i>t</i> = 3.541, <i>df</i> = 4.000 | IBA1 ⁺ in EPL | 0.023985 | | |
| | | <i>t</i> = 3.989, <i>df</i> = 4.000 | IBA1 ⁺ in GCL | 0.016275 | | |
| | | <i>t</i> = 2.878, <i>df</i> = 4.000 | IBA1 ⁺ in RMS | 0.045123 | | |
| | | <i>t</i> = 12.46, <i>df</i> = 4.000 | IBA1 ⁺ in PC - total (average) | 0.000239 | | |
| | | <i>t</i> = 8.485, <i>df</i> = 4.000 | IBA1 ⁺ in PC - LOT | 0.001058 | | |
| Microglia counts in PC and TuS (Fig. 6) | Multiple unpaired <i>t</i> tests | <i>t</i> = 10.85, <i>df</i> = 4.000 | IBA1 ⁺ in PC - L1 | 0.000409 | | |
| | | <i>t</i> = 19.35, <i>df</i> = 4.000 | IBA1 ⁺ in PC - L2 | 0.000042 | | |
| | | <i>t</i> = 9.483, <i>df</i> = 4.000 | IBA1 ⁺ in PC - L3 | 0.000690 | | |
| | | <i>t</i> = 6.632, <i>df</i> = 4.000 | IBA1 ⁺ in TuS - total (average) | 0.002681 | | |
| | | <i>t</i> = 4.255, <i>df</i> = 4.000 | IBA1 ⁺ in TuS - L2 | 0.013110 | | |
| | | <i>t</i> = 4.834, <i>df</i> = 4.000 | IBA1 ⁺ in TuS - L3 | 0.008437 | | |
| | | <i>t</i> = 6.042, <i>df</i> = 4.000 | CNPase pixels LOT | 0.003785 | | |
| | | <i>t</i> = 5.229, <i>df</i> = 4.000 | CNPase pixels AC | 0.006389 | | |
| | | Average pixel intensity CNPase (Fig. 7) | Multiple unpaired <i>t</i> tests | <i>t</i> = 6.042, <i>df</i> = 4.000 | CNPase pixels LOT | 0.003785 |
| | | | | <i>t</i> = 5.229, <i>df</i> = 4.000 | CNPase pixels AC | 0.006389 |

Results

Distribution of SARS-CoV-2-infected cells across the OS

We examined cells targeted by SARS-CoV-2 in the OS in K18hACE2 mice, which expresses human ACE2 under the cytokeratin-18 promoter. At 7 d postinfection, we quantified their distribution across the different regions of the OS. OSNs have the initial exposure to SARS-CoV-2 following intranasal inoculation of the virus, followed by three regions in the CNS: the OB, the PC, and the TuS, formerly known as the olfactory tubercle (Wesson, 2020; Fig. 1A).

The OE is anatomically separated into the medial septum and the lateral turbinates, the latter of which has been suggested to be more sensitive to viruses (Urata et al., 2021). Here, we found that SARS-CoV-2 nucleocapsid-positive cells were sparsely distributed in both the septum and the turbinates. Uninfected mice showed no labeling with SARS-CoV-2-nucleocapsid (NC; data not shown). Infected cells had a polygonal morphology resembling SC and occurred individually or in small clusters of ~10 cells (Fig. 1B,B'). The numbers of SARS-CoV-2⁺ cells did not differ between the septum and turbinates (Fig. 1b). In the OB, the majority of SARS-CoV-2⁺ cells were found in the MCL-IPL, where the largest projection neurons of the OB (mitral cells) are located (Fig. 1C,c). Fewer cells were found in the superficial ONL, as well as in the region of the GL and EPL where tufted cells, the second population of OB projection neurons, are located (Fig. 1C,c). In the EPL, some blood vessels were labeled for SARS-CoV-2 nucleocapsid (Fig. 1C, arrowheads), suggesting that endothelial cells were also targeted by the virus.

The cortical (PC) and subcortical (TuS) regions of the OS are the main areas of the brain receiving direct input from the OB. Both are arranged in layers and are innervated by the axons coming from the OB that form the LOT. In PC, these layers are as follows: a plexiform Layer 1, where the LOT axons make synapses with the apical dendrites of projection neurons; a densely packed Layer 2, where the projection neuron somata are located; and a thicker but less dense Layer 3 (Martin-Lopez et al., 2019a,b). Here, most infected cells were pyramidal/projection neurons located in Layers 2 and 3 (Fig. 1D,d), resembling the infections reported in neocortical pyramidal neurons (Golden et al., 2020; Vidal et al., 2022). Deep into the LOT, some SARS-CoV-2⁺ were occasionally observed in the superficial Layer 1 (Fig. 1D), likely belonging to local

circuit horizontal cells (Neville and Haberly, 2004). In TuS, most SARS-CoV-2⁺ cells corresponded to projection neurons from Layers 2 and 3 (Fig. 1E,e).

Interestingly, the cytoarchitecture and morphology of all OS regions remained intact in infected animals, as previously reported in laboratory animals (Dedoni et al., 2022), suggesting that damage to the OS is likely concentrated at the molecular level. The mice employed in this study express the hACE2 protein under the control of the K18 promoter. Expression of K18 is found predominately in epithelial cells and not the brain (Abe and Oshima, 1990; McCray et al., 2007; Dedoni et al., 2022). Thus, the expression of hACE2 in the brain is almost undetectable. Nevertheless, our results established that SARS-CoV-2 did infect SC in the periphery and neurons across all areas of the central OS, suggesting the likely neurotropism of this virus under certain conditions of severe infection.

Characterization of SARS-CoV-2-infected cells

Next, we sought to investigate the cellular phenotypes of those cells that showed an affinity for SARS-CoV-2 infection throughout the different OS regions. The OE lines the posterior part of the nasal cavity and includes three primary epithelial cells (Harkema et al., 2006; Fig. 2A): (1) the OSNs; (2) SC; and (3) basal cells which are the OE neural stem cells. In mice, OSNs are characterized by their exclusive expression of olfactory marker protein (OMP) (Farbman and Margolis, 1980) and only 1 of the ~1,200 odorant receptors (Vassar et al., 1993). The SCs are columnar epithelial cells that surround the OSNs and provide them with support and nutrients. SCs can be identified with the expression of cytokeratin-8 (CK8; Maurya et al., 2015). The basal cells lie next to the lamina propria and are subdivided into horizontal basal cells that express cytokeratin-5 (Maurya et al., 2015) and globose basal cells that express Sox2 (Guo et al., 2010). Our results showed that SARS-CoV-2⁺ cells in the OE belonged to two different populations: (1) cells that exhibited an elongated and polygonal cell shape that extended from the apical surface to the lamina propria of the OE, expressing CK8 but not OMP (Fig. 2B–b’), identified as SC, and (2) macrophages lying over the lamina propria that expressed IBA1, a marker characteristic of the monocyte/macrophage lineages (Fig. 2C–c’). Basal cells expressing Sox2 were not infected with SARS-CoV-2 (data not shown). The preferential infection of SC by SARS-CoV-2 aligns with previous reports in both laboratory animals and humans (Cantuti-Castelvetri et al., 2020; Khan et al., 2021; Ye et al., 2021; Finlay et al., 2022; Verma et al., 2022; Zazhytska et al., 2022). However, we pioneered in finding infection only from macrophages in the OE lamina propria.

Across the OB layers (Fig. 2D), most SARS-CoV-2⁺ cells were found in the MCL-IPL which colocalized with the marker Reelin (Reln; Fig. 2E–e’). Reln is characteristic of OB projection neurons, mitral and tufted cells (M/Tc), which are found in the MCL-IPL and EPL (Martin-Lopez et al., 2011). Similar results were observed with those cells located in the deep GL and superficial EPL (data not shown). Reln has, however, been implicated in hyperinflammatory responses in epithelial cells in COVID-19 patients (Calvier et al., 2023). Since there is evidence for ACE2 coexpression with furin in the GL and MCL (Ueha et al., 2021), our data align with the hypothesis that under the specific conditions of severe disease, SARS-CoV-2 is able to infect M/Tc, possibly using ACE2/furin as entry protein receptors. In the ON, where OSN axons enter the OB, some SARS-CoV-2⁺ cells were found coexpressing the marker IBA1 and were identified as infected microglia (Fig. 2G–g’). Blood vessels were frequently labeled with SARS-CoV-2-NC in the EPL (Fig. 2F).

In PC and TuS, SARS-CoV-2 was found labeling only neurons and not microglial cells. The PC is a trilaminar cortex deep into the LOT and acts as the primary and associational olfactory cortex (Fig. 2H). Here, projection neurons are glutamatergic and express Tbr1 and Ctip2 (Martin-Lopez et al., 2019a,b). Both markers were coexpressed with SARS-CoV-2-NC⁺ in neurons of Layers 2 and 3 in K18hACE2 mice (Fig. 2I–i’). In Layer 1, some horizontal cells were also infected with SARS-CoV-2, and although they are presumed to be GABAergic interneurons (Shepherd et al., 2021), they also expressed the marker Ctip2 (Fig. 2J–j’). The expression of Ctip2 by GABAergic neurons is characteristic of projection neurons in the TuS Layers 2 and 3, which do not express the cortical marker Tbr1 (Martin-Lopez et al., 2019b). Our data in the TuS demonstrated that SARS-CoV-2⁺ cells were located in Layers 2 and 3 and in the islands of Calleja, all expressing Ctip2 (Fig. 2K,L–l’).

Collectively, these data confirmed that under conditions of acute disease in the K18hACE2 mice, SARS-CoV-2 targets SC and macrophages in the OE, while it showed neurotropism for projection neurons in the OB, PC, and TuS. Some microglial cells were also labeled with SARS-CoV-2-NC in the ONL and blood vessels in the EPL inside the OB. Since OSNs were not labeled with SARS-CoV-2-NC in the OE, which are the only cells connected to M/Tc through the olfactory nerve, axonal transport seems unlikely, and we support the hypothesis of a different entry route into the CNS likely using a hematopoietic pathway (Awogbindin et al., 2021; Tsukahara et al., 2023).

Microglial activation in response to SARS-CoV-2

During inflammation of the CNS, activated microglia proliferate in a process known as microgliosis (Zabel and Kirsch, 2013; Borst et al., 2021). After SARS-CoV-2 infections, microgliosis is well documented in both humans and laboratory animals (Poloni et al., 2021; Fernandez-Castaneda et al., 2022; Kaufner et al., 2022; Kishimoto-Urata et al., 2022; Olivaria et al., 2022; Dey and Bishayi, 2023). We first assessed the morphological changes associated with microgliosis by using a fractal analysis of individual cells in PC as previously described (Soltys et al., 2001; Meller et al., 2023). We searched for resting states, identified by small round cell bodies that extend highly branched thin processes (ramified microglia), and activated microglia, whose morphology become amoeboid and hypertrophic, characterized by large

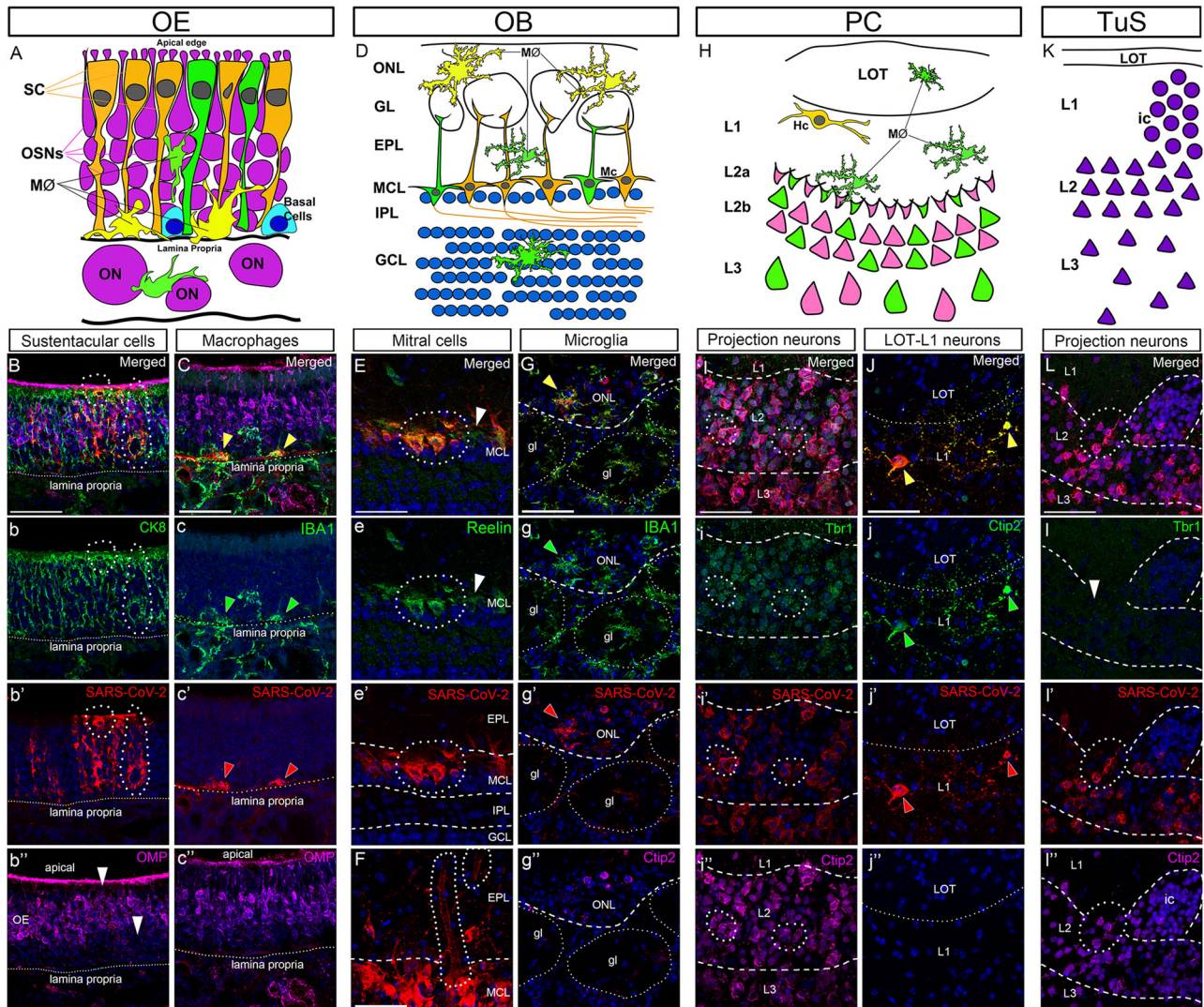


Figure 2. Molecular characterization of SARS-CoV-2-infected cells. **A**, Diagram illustrating the main cell types of the OE. **B–b''**, IHC in the OE detecting the SC marker CK8 (**b**, green), SARS-CoV-2-NC (**b'**, red) and OSN marker OMP (**b''**, magenta). SARS-CoV-2-NC⁺ cells colocalize with CK8 (**B**) but not with OMP (**b''**, arrowheads). **C–c''**, IHC in the OE staining for the macrophage marker IBA1 (**c**, green), SARS-CoV-2-NC (**c'**, red), and OMP (**c''**, magenta), showing infected macrophages lying in the lamina propria (arrowheads). **D**, Diagram illustrating the layers and main cell types of the OB. **E–e''**, IHC in the OB staining for Reln (**e**, green) and SARS-CoV-2-NC (**e'**, red). All SARS-CoV-2-NC⁺ cells in the MCL express Reln (**E**, **e**), confirming their phenotype as infected mitral cells. **F**, SARS-CoV-2-NC⁺ labeling in blood vessels from the EPL. **G–g''**, IHC staining for IBA1 (**g**, green), SARS-CoV-2-NC (**g'**, red), and Ctip2 (**g''**, magenta), showing infected microglial cells in the ONL (**G–g'**, arrowheads). **H**, Diagram illustrating the layers and main cell types of the PC. **I–i''**, IHC in PC staining for Tbr1 (**i**, green), SARS-CoV-2-NC (**i'**, red), and Ctip2 (**i''**, magenta). All neurons from Layers 2 and 3 are found to coexpress SARS-CoV-2-NC⁺ with Tbr1 (**I**, **i**, dotted lines) and Ctip2 (**I'**, **i''**, dotted lines) confirming they are projection neurons. **J–j''**, IHC staining to detect Ctip2 (**j**, green) and SARS-CoV-2-NC (**j'**, red) showing that Hc from the superficial Layer 1 are infected with SARS-CoV-2 (arrowheads). **K**, Diagram illustrating the layers and of the TuS. **L–l''**, IHC in TuS staining for Tbr1 (**l**, green), SARS-CoV-2-NC (**l'**, red), and Ctip2 (**l''**, magenta) showing the absence of Tbr1 expression in the entire TuS and coexpression of SARS-CoV-2-NC with Ctip2 highlighting the virus targeting projection neurons in the TuS. Nuclei counterstained with DAPI (blue). CK8, cytokeratine-8; Ctip2, COUP-TF-interacting protein 2; gl, glomeruli; Hc, horizontal cell; ic, island of Calleja; IHC, immunohistochemistry; LOT, lateral olfactory tract; MØ, microglia; Mc, mitral cells; OB, olfactory bulb; OE, olfactory epithelium; OMP, olfactory marker protein; OSN, olfactory sensory neurons; PC, piriform cortex; RMS, rostral migratory stream; SC, supporting/sustentacular cells; Tbr1, T-Box brain transcription Factor 1; TuS, tubular striatum. Scale bar, 50 µm.

cell bodies with shorter thicker processes (Blackbeard et al., 2007; Lier et al., 2021). Microglia were identified with the marker IBA1, characteristic of monocyte–macrophage lineages.

After 7 d of infection with SARS-CoV-2, most microglial cells in PC showed an activated state (Fig. 3A–C) as described in the neocortex (Villadiego et al., 2023). This effect may be unique for coronaviruses, since brain infections with other viruses, such as influenza, do not induce changes in microglia morphology (Dusedau et al., 2021). In the OE, changes in macrophage morphology were not analyzed since those changes have not yet been fully characterized in vivo, and it is believed that they change gradually in a spectrum of different elongated states (McWhorter et al., 2013).

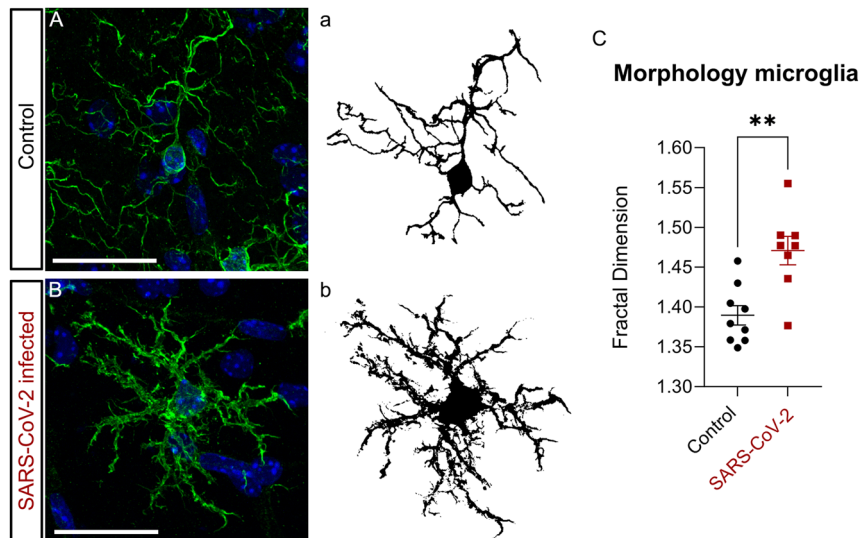


Figure 3. Morphology of activated microglia. Immunostaining for the microglial marker IBA1 (green) with nuclei counterstained with DAPI (blue). **A, a**, Morphology of microglia in control animals. **B, b**, Morphology of microglia in infected animals. **C**, Microglia changes in morphology in response to SARS-CoV-2 infection to show a statistically significant increase in the fractal dimension in infected mice. Statistics: unpaired *t* test with $** = p < 0.01$ (Table 2). Scale bar, 25 μm .

Microgliosis and macrophage activation in the OS induced by SARS-CoV-2

Next, we studied macrophages (in the periphery) and microglia (within the CNS) proliferation by quantifying their numbers along the different OS regions, as well as their phagocytic activity. Phagocytic macrophages/microglia were assessed by labeling with the marker C-type lectin domain family 7 member A or Dectin-1 (Clec7A; Krasemann et al., 2017). Infectious diseases targeting neural regions lead to activation of the monocyte/macrophage lineages resulting in strong inflammation (Hoogland et al., 2015; Merad et al., 2022). Macrophages/microglial cells were identified with IBA1, while those actively phagocytosing were identified with the coexpression of IBA1⁺/Clec7A⁺. We colabeled with SARS-CoV-2-NC to determine if inflammatory cells clustered around infected cells.

In the OE, there was an overall increase in the total number of macrophages that was significantly higher in the septum of infected mice (Fig. 4C). The increase in the turbinates was evident but not statistically significant (Fig. 4C). The number of phagocytic macrophages (IBA1⁺/Clec7A⁺) showed no statistically significant differences between controls and infected mice (Fig. 4A,B, arrowheads; C). The significant increase in the number of IBA1⁺ macrophages in the septum suggested this region may be more vulnerable to inflammation than the turbinates, even though both regions were equally infected by the virus (Fig. 1b). These data contrast with that of others who suggested a higher sensitiveness of the turbinates (Kaufer et al., 2022; Ueha et al., 2022). No clustering of macrophages was evident around SARS-CoV-2⁺ cells.

In the OB, the total number of microglia (IBA1⁺) and phagocytic microglia (IBA1⁺/Clec7A⁺) was significantly higher in infected animals, suggesting an enhanced inflammatory response to the presence of the virus (Fig. 5A–C). Quantifications were made by OB layers to detect whether the inflammation in the OB occurred predominantly in those layers where we detected the virus (Fig. 1C,c). Unexpectedly, our data showed microglial numbers were significantly higher across all layers of the OB with the exception of the MCL-IPL (Fig. 5C). The number of phagocytic microglia was significantly higher in infected animals only in the GL (Fig. 5C). Infected microglia were also evident in the adjacent ONL (Fig. 5B, dotted lines), where OSN axons reach the OB. These data suggested that microgliosis was independent of the location of the infected cells.

Finally, in PC and TuS, microgliosis was widely distributed. In PC we found a significant increase in the total number of microglial cells across all layers of PC, showing an evident change to an activated cell morphology (Fig. 6A_(PC), B_(PC), C). Unexpectedly, the number of phagocytic microglia was almost undetectable, showing a slight, but not significant, increase across the layers. Similarly, in TuS we observed microgliosis predominantly in the densely packed cell Layers 2 and 3 (Fig. 6A_(TuS), B_(TuS), D). Although we did not quantify cells in other areas of the brain, it was evident that microgliosis was widespread within the CNS of infected animals (Fig. 6B) as previously reported (Golden et al., 2022; Olivaria et al., 2022; Seehusen et al., 2022).

Disruptions in myelin integrity caused by SARS-CoV-2

In the CNS, the regulation of axon–oligodendroglia interactions is essential to maintain the integrity of the myelin sheaths. In mature myelinated tracts, the enzyme CNPase plays a critical role in maintaining a healthy myelin–axon

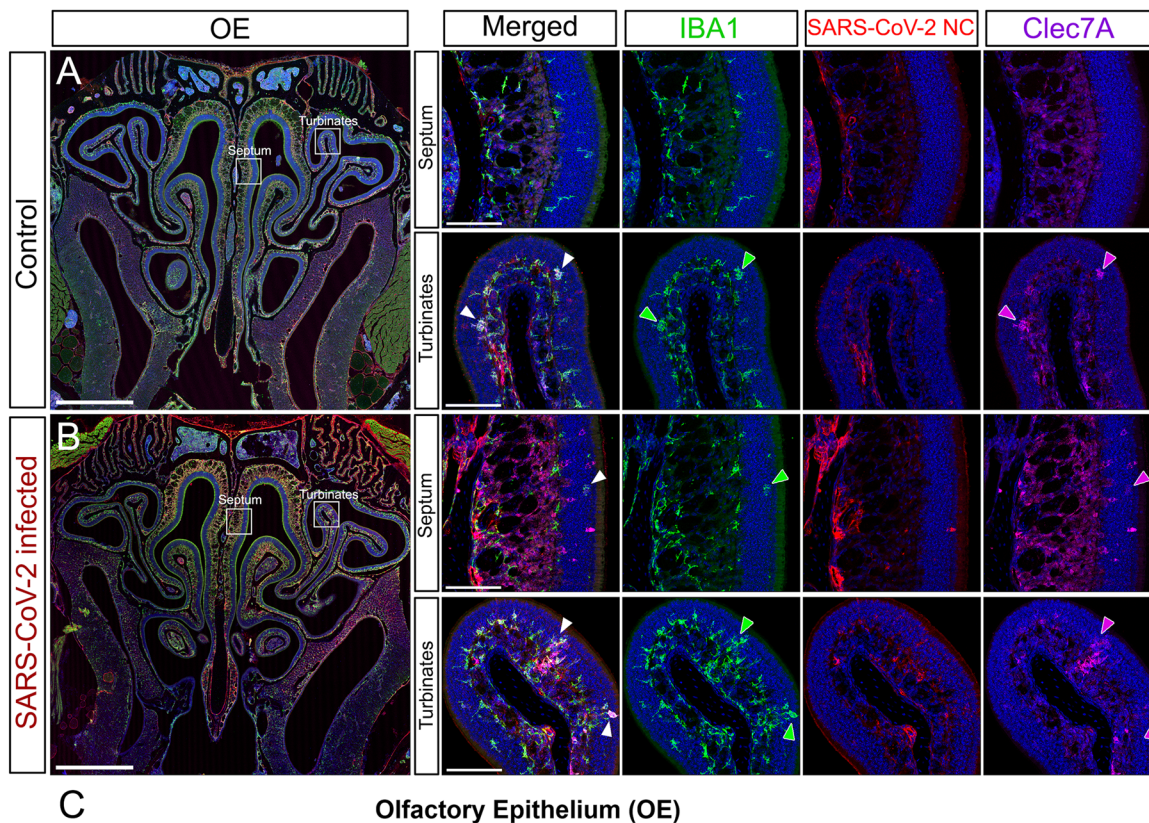


Figure 4. Microgliosis in the OE. Staining of the OE with the macrophage marker IBA1 (green), SARS-CoV-2 nucleocapsid (red), and active phagocytic macrophages Dectin-1 (Clec7A; magenta). Nuclei counterstained with DAPI (blue). **A** with insets, Representative images of the OE from control mice. **B** with insets, Representative images of the OE from SARS-CoV-2-infected mice. **C**, Quantification of total macrophage cells (IBA1⁺) and phagocytic macrophages (IBA1⁺/Clec7A⁺) in the medial wall (septum) and turbinates. The number of combined IBA1⁺ cells between the septum and turbinates shows an increase that was statistically significant only in the septum (**C**), suggesting a higher vulnerability of this region to the infection. Statistics: multiple unpaired *t* test with * = *p* < 0.05 (Table 2). Scale bars: **A** and **B**, 1 mm; septum and turbinate insets, 100 μ m.

interface (Lappe-Siefke et al., 2003). Some evidence suggests that SARS-CoV-2 has an impact on the brain myelin that could explain some of the neurological symptoms displayed by COVID-19 patients (Domingues et al., 2020; Poloni et al., 2021; Fernandez-Castaneda et al., 2022). In this work, we measured the CNPase levels in the two main OS myelinated tracts, the LOT and the AC, to examine myelin damages in the K18hACE2 mouse model of COVID-19. Our analyses revealed that there was a statistically significant reduction of CNPase in both the LOT and the AC (Fig. 7A–E) after 7 d of infection, suggesting a loss of myelin and altered axonal conduction.

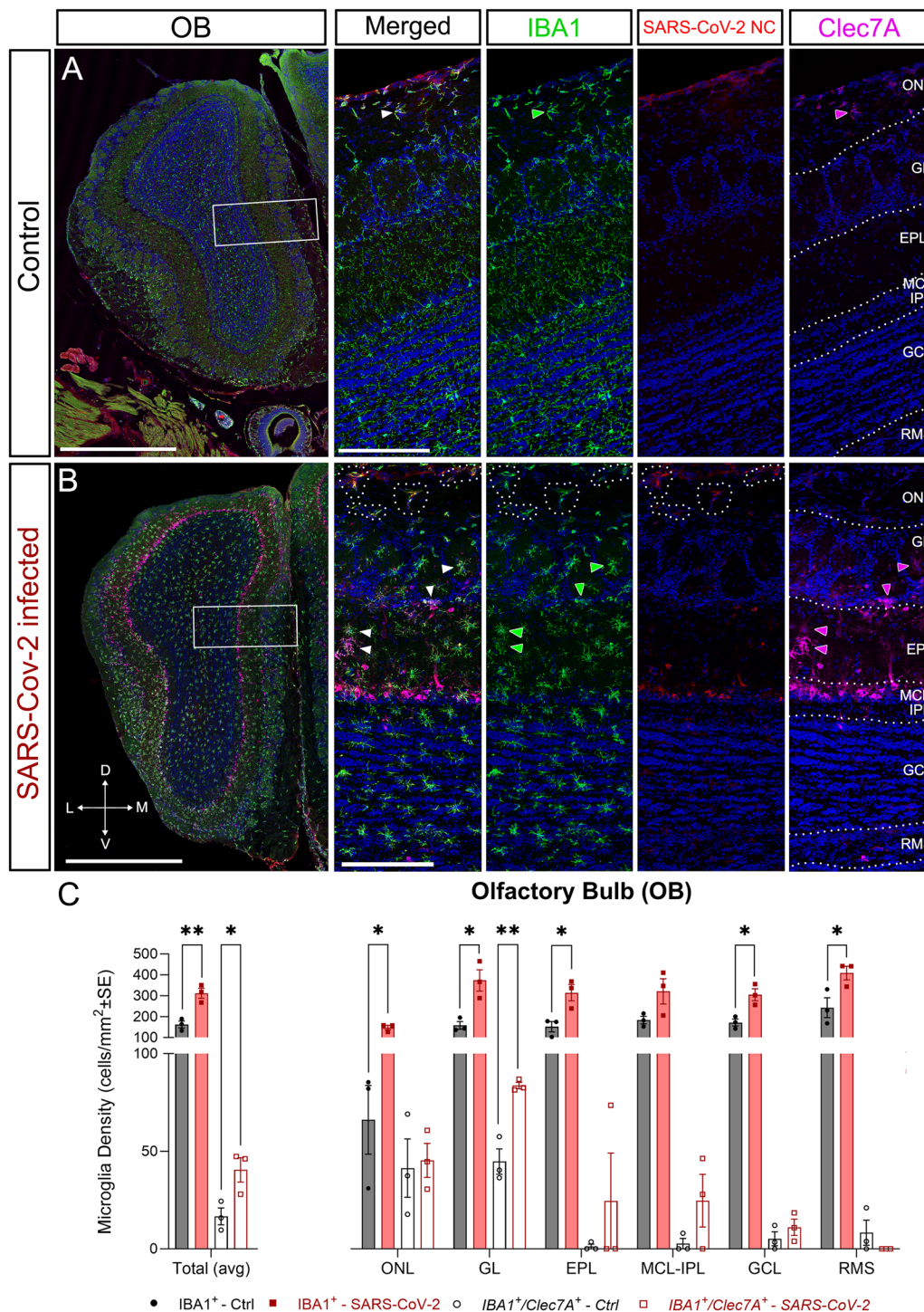


Figure 5. Microgliosis in the OB. Staining of microglia with IBA1 (green), SARS-CoV-2 nucleocapsid protein (red), and active phagocytic microglia with Dectin-1 (Clec7A; magenta). Nuclei counterstained with DAPI (blue). **A**, Representative images of the OE from control mice. **B**, Representative images of the OE from SARS-CoV-2-infected mice. Microglial cell bodies show a clear hypertrophy related to an activated response. Infected microglia are observed in the ONL (dotted lines). **C**, Quantification of the microglia (IBA1⁺) and phagocytic microglia (IBA1⁺/Clec7A⁺) in the OB. Total numbers of microglia (IBA1⁺) are statistically significant higher numbers in infected animals, suggesting a strong inflammation. This effect is replicated on each individual layer excepting in the MCL-IPL, which is the layer less affected by the microgliosis. Numbers of phagocytic microglia (IBA1⁺/Clec7A⁺) are significantly higher only in the GL, indicating that this layer is the most affected by inflammation. EPL, external plexiform layer; GCL, granule cell layer; GL, glomerular layer; IPL, internal plexiform layer; MCL, mitral cell layer; OB, olfactory bulb; ONL, olfactory nerve layer; RMS, rostral migratory stream (bulbar part). Statistics: multiple unpaired *t* test with * = *p* < 0.05; ** = *p* < 0.01 (Table 2). Scale bars: **A** and **B**, 1 mm; high magnification insets, 200 μm.

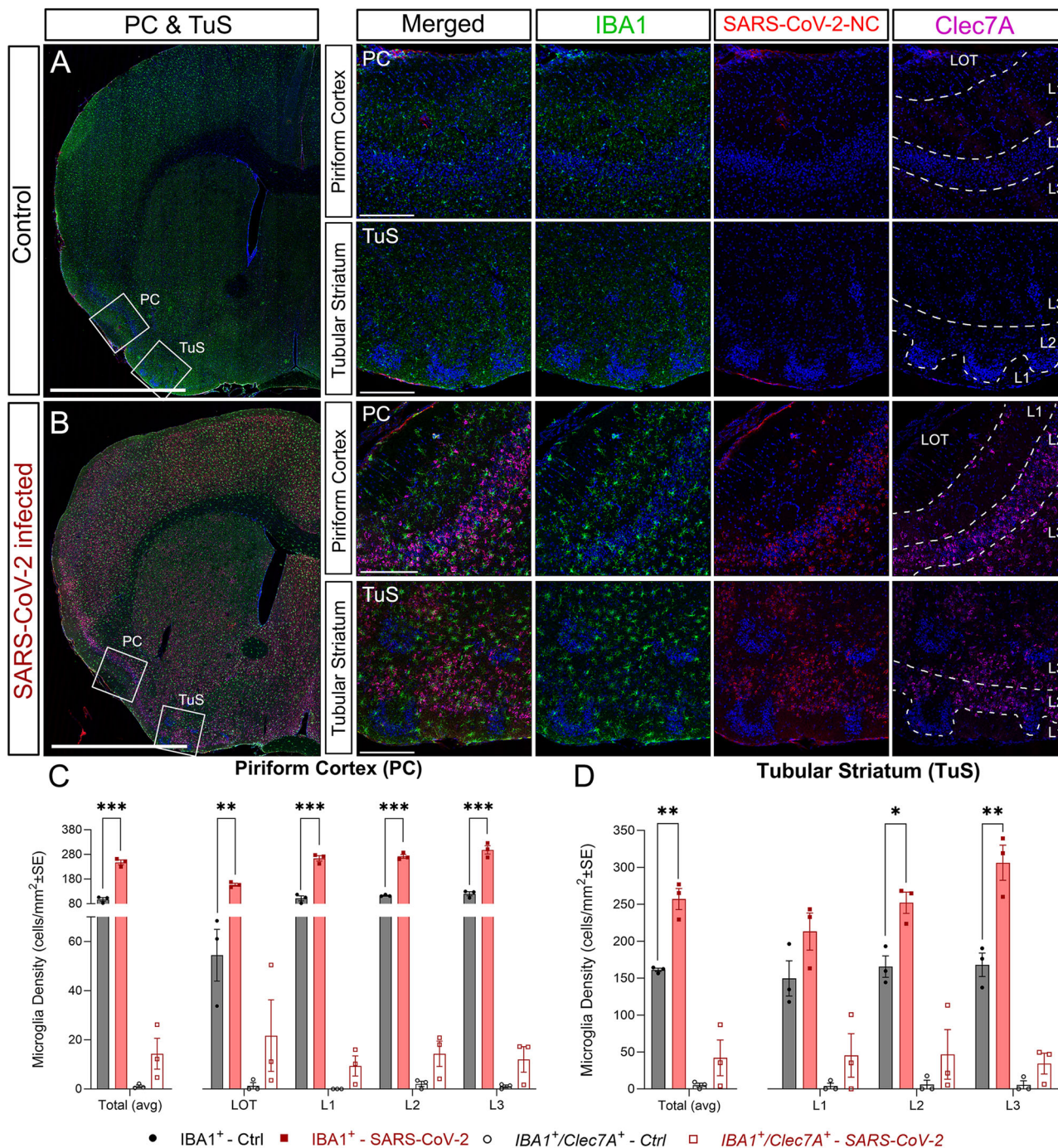


Figure 6. Microgliosis in piriform cortex and TuS. Staining of microglia with IBA1 (green), SARS-CoV-2 nucleocapsid (red), and active phagocytic macrophages with Dectin-1 (Clec7A; magenta). Nuclei counterstained with DAPI (blue). **A**, Representative images of the PC and TuS from control mice. **B**, Representative images of the PC and TuS from SARS-CoV-2-infected mice, where clear hypertrophy is observed in all cell bodies extending not only into the PC and TuS but also across the entire brain. **C**, Quantification of microglia (IBA1⁺) and phagocytic microglia (IBA1⁺/Clec7A⁺) in PC. The numbers of microglia are statistically significantly higher in all layers of PC from infected animals proving the presence of strong inflammation. **D**, Quantification of microglia (IBA1⁺) and phagocytic microglia (IBA1⁺/Clec7A⁺) in TuS. The numbers of microglia (IBA1⁺) were significantly higher in Layers 2 and 3 highlighting that inflammation affected the projection neuron layers. Numbers of phagocytic microglia (IBA1⁺/Clec7A⁺) are similar in both controls and infected mice. LOT, lateral olfactory tract; PC, piriform cortex; TuS, tubular striatum. Statistics: multiple unpaired *t* test with * = *p* < 0.05; ** = *p* < 0.01; *** = *p* < 0.001 (Table 2). Scale bars: **A** and **B**, 1 mm; high magnification insets, 200 μm.

Discussion

The awareness of sense of smell during our daily life changed dramatically in 2019 with the emergence of a new strain of coronavirus that caused the COVID-19 disease. At the beginning of the pandemic, the number of people infected with

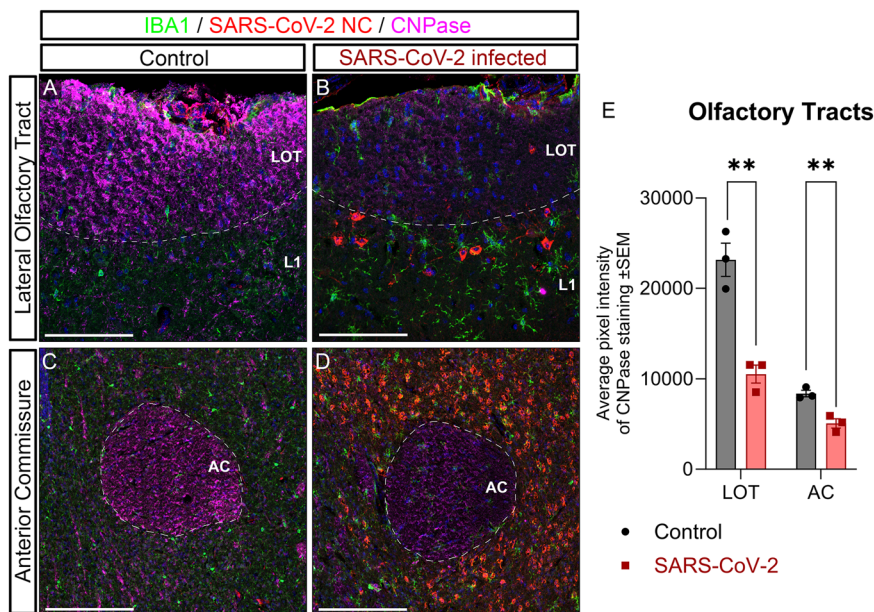


Figure 7. Myelination defects in the LOT and AC. **A–D**, Staining of microglia with IBA1 (green), SARS-CoV-2 nucleocapsid (red), and CNPase (magenta). Nuclei counterstained with DAPI (blue). **A**, Representative images of IHC staining in the LOT of control and infected mice. **B**, Representative images of IHC staining in the AC of control and infected mice. **E**, Quantification of the CNPase pixel intensity shows a statistically significant decrease in the intensity for both, the LOT and AC in SARS-CoV-2-infected mice compared with those in controls. AC, anterior commissure; LOT, lateral olfactory tract. Statistics: multiple unpaired *t* test with ****** = $p < 0.01$ (Table 2). Scale bar, 100 μ m.

SARS-CoV-2 that reported some level of olfactory dysfunction exceeded 80% (Cooper et al., 2020; Lechien et al., 2020). These numbers pointed to the OS as one of the main targets of the virus. Most evidence suggests that compromise of the SC is the main reason for direct or indirect damages to the OSNs that produce olfactory dysfunction (Khan et al., 2021, 2022; Finlay et al., 2022; Zazhytska et al., 2022; Ziuzia-Januszewska and Januszewski, 2022; Tsukahara et al., 2023). However, although the findings remain controversial, there are some data suggesting that SARS-CoV-2 can infect neurons in the OS and therefore contribute to the perturbation of olfactory function. To shed new light on this paradigm, we used the K18hACE2 mice to study the viral infection and inflammation in the OS, especially in the central regions OB, PC, and TuS (Yinda et al., 2021; Zheng et al., 2021; Dong et al., 2022; S. Choi et al., 2024).

Our analysis in the OE confirmed that SC are the only cell type susceptible to infection in the OE of K18hACE2 mice, consistent with reports of human pathology (Bryche et al., 2020; Cantuti-Castelvetri et al., 2020; Khan et al., 2021; Ye et al., 2021; Finlay et al., 2022; Verma et al., 2022; Zazhytska et al., 2022). These findings were expected since SCs are the only cells expressing the tandem proteins ACE2/TMPRSS2 used by SARS-CoV-2 as entry cell molecules (Bilinska et al., 2020; Brann et al., 2020; Fodouliau et al., 2020). Our data support the hypothesis that direct damage to OSNs is unlikely to explain loss of smell, as some have proposed (Sia et al., 2020; Meinhardt et al., 2021; Ziuzia-Januszewska and Januszewski, 2022; Shimizu et al., 2024). In addition to SARS-CoV-2 infection in the OE, we found that inflammation was more prominent in the septum compared with that in the turbinates unlike prior reports (Golden et al., 2020, 2022; Kumari et al., 2021; Ueha et al., 2022). We speculate that SC in the septum may exhibit different topographically defined molecular phenotypes as occurs with the OSNs (Zapiec and Mombaerts, 2020) that could make them to be more susceptible of infection. We also found that macrophages in the lamina propria of the OE were infected by SARS-CoV-2, but not those that were distributed throughout the thickness of the OE or internal to the lamina propria (Fig. 2C–c'). The ability of SARS-CoV-2 to infect cells from the monocyte/macrophage lineages is known (Jeong et al., 2022; Eberhardt et al., 2023), but here we demonstrate for the first time that only those macrophages aligned to the lamina propria were infected. IBA1⁺ cells arranged along the lamina propria were reported to be proximal to infected SC, but they were never infected with SARS-CoV-2 (Bourgon et al., 2022). In our tissues, none of these macrophages were found proximal to SC-infected cells that could explain a cell-to-cell transference of viral particles. This possibility would benefit from further research addressing the vulnerability of IBA1⁺ cells in the OE to SARS-CoV-2 infections.

However, despite the damage to the epithelium, the question regarding the possibility of the virus infecting neurons within the CNS that could contribute to olfactory deficits, particularly those causing long-term loss of olfaction, remains unanswered. While Meinhardt et al. (2024) speculate on indirect effects on neurons (Meinhardt et al., 2024), there is also evidence that support direct neuronal damage caused by the virus. For example, Esposito et al. (2022, 2023) reported anomalies in cortical connectivity and function following SARS-CoV-2 infections. In support of a CNS pathology, SARS-CoV-2 RNA has been reported in brain biopsies from COVID-19 patients (Matschke et al., 2020; Meinhardt

et al., 2021). Finally, damage in the myelin sheath of CNS axons is well documented both here and previously and could contribute to neurological symptoms including impaired olfactory function (Garg et al., 2021; Fernandez-Castaneda et al., 2022). These data represent examples of damages in the CNS that, at least in some patients, involve some degree of neuronal infection by SARS-CoV-2 that may host replicating viral particles inside the cells.

Interestingly, within the OB, the virus infected the projection neurons M/Tc, which was most likely the result of their coexpression of furin with murine ACE2, which have been suggested to be alternative SARS-CoV-2 entry receptors (Ueha et al., 2021). It seems reasonable to speculate and open for discussion the possibility that the infection of other projection neurons throughout the brain was associated with the expression of other proteins used by the virus as entry receptors that are independent of ACE2 or TMPRSS2 (Iadecola et al., 2020; Zhao and Gao, 2024).

In accordance with previous work, we found significantly higher numbers of microglia in all OS regions (OB, PC, and TuS) suggesting widespread neuroinflammation (Awogbindin et al., 2021; Savelieff et al., 2022; Vidal et al., 2022). However, others have reported an increase in the OB but not in PC (Kaufer et al., 2022); an increase only in PC (Carossino et al., 2022); no changes at all (Fernandez-Castaneda et al., 2022); or reductions in the numbers of microglia (Jeong et al., 2022). While the question remains to be resolved, it seems that the most parsimonious explanation would include microgliosis accompanying the SARS-CoV-2 infections and accounting, at least in part, for the associated neurological symptoms. Limitations of this study include the use of transgenic mice as a model for human disease, which may not recapitulate precisely the pathology seen in infected humans, and the use of only the ancestral isolate of SARS-CoV-2, which may not represent the pathology of more recent variants of concern.

In summary, we found that SARS-CoV-2 infections in the K18hACE2 mouse infected SC and lamina propria macrophages in the OE, but not OSNs. In the CNS, SARS-CoV-2 infected microglial cells in the ONL of the OB and projection neurons in all OS regions (OB, PC, and TuS). The most obvious alteration that we observed was a widespread microgliosis throughout the brain and damage to integrity of the myelin in the LOT and the AC. However, there were no evident disturbances to the cytoarchitecture in these regions suggesting that damages may reside at the molecular level. Our data support the hypothesis that the neuronal infection likely occurred through infected microglial cells used as a “Trojan horse” to infect neurons as has been previously proposed (Awogbindin et al., 2021). Collectively, these findings contribute to our understanding of the olfactory deficits in both humans and animal models with SARS-CoV-2 infections. Therefore, therapies designed to target the virus entry points, such as the use of vaccines that induce a humoral response producing blocking antibodies of the spike protein, seems to be the safest approach to ensure protection against brain infection.

References

- Abe M, Oshima RG (1990) A single human keratin 18 gene is expressed in diverse epithelial cells of transgenic mice. *J Cell Biol* 111:1197–1206.
- Awogbindin IO, Ben-Azu B, Olusola BA, Akinluyi ET, Adeniyi PA, Di Paolo T, Tremblay ME (2021) Microglial implications in SARS-CoV-2 infection and COVID-19: lessons from viral RNA neurotropism and possible relevance to Parkinson's disease. *Front Cell Neurosci* 15:670298.
- Beckman D, et al. (2022) SARS-CoV-2 infects neurons and induces neuroinflammation in a non-human primate model of COVID-19. *Cell Rep* 41:111573.
- Bergmann CC, Silverman RH (2020) COVID-19: coronavirus replication, pathogenesis, and therapeutic strategies. *Cleve Clin J Med* 87:321–327.
- Bilinska K, Butowt R (2020) Anosmia in COVID-19: a bumpy road to establishing a cellular mechanism. *ACS Chem Neurosci* 11:2152–2155.
- Bilinska K, Jakubowska P, Von Bartheld CS, Butowt R (2020) Expression of the SARS-CoV-2 entry proteins, ACE2 and TMPRSS2, in cells of the olfactory epithelium: identification of cell types and trends with age. *ACS Chem Neurosci* 11:1555–1562.
- Blackbeard J, O'Dea KP, Wallace VC, Segerdahl A, Pheby T, Takata M, Field MJ, Rice AS (2007) Quantification of the rat spinal microglial response to peripheral nerve injury as revealed by immunohistochemical image analysis and flow cytometry. *J Neurosci Methods* 164:207–217.
- Blume C, et al. (2021) A novel ACE2 isoform is expressed in human respiratory epithelia and is upregulated in response to interferons and RNA respiratory virus infection. *Nat Genet* 53:205–214.
- Borst K, Dumas AA, Prinz M (2021) Microglia: immune and non-immune functions. *Immunity* 54:2194–2208.
- Bourgon C, Albin AS, Ando-Grard O, Da Costa B, Domain R, Korkmaz B, Klonjowski B, Le Poder S, Meunier N (2022) Neutrophils play a major role in the destruction of the olfactory epithelium during SARS-CoV-2 infection in hamsters. *Cell Mol Life Sci* 79:616.
- Brann DH, et al. (2020) Non-neuronal expression of SARS-CoV-2 entry genes in the olfactory system suggests mechanisms underlying COVID-19-associated anosmia. *Sci Adv* 6:eabc5801.
- Brodin P (2021) Immune determinants of COVID-19 disease presentation and severity. *Nat Med* 27:28–33.
- Bryche B, et al. (2020) Massive transient damage of the olfactory epithelium associated with infection of sustentacular cells by SARS-CoV-2 in golden Syrian hamsters. *Brain Behav Immun* 89:579–586.
- Burks SM, Rosas-Hernandez H, Alejandro Ramirez-Lee M, Cuevas E, Talpos JC (2021) Can SARS-CoV-2 infect the central nervous system via the olfactory bulb or the blood-brain barrier? *Brain Behav Immun* 95:7–14.
- Butowt R, Bilinska K, von Bartheld CS (2023) Olfactory dysfunction in COVID-19: new insights into the underlying mechanisms. *Trends Neurosci* 46:75–90.
- Butowt R, Meunier N, Bryche B, von Bartheld CS (2021) The olfactory nerve is not a likely route to brain infection in COVID-19: a critical review of data from humans and animal models. *Acta Neuropathol* 141:809–822.
- Calvier L, Drelich A, Hsu J, Tseng CT, Mina Y, Nath A, Kounnas MZ, Herz J (2023) Circulating Reelin promotes inflammation and modulates disease activity in acute and long COVID-19 cases. *Front Immunol* 14:1185748.
- Cantuti-Castelvetri L, et al. (2020) Neuropilin-1 facilitates SARS-CoV-2 cell entry and infectivity. *Science* 370:856–860.

- Cappelletti G, et al. (2023) Human motor neurons derived from induced pluripotent stem cells are susceptible to SARS-CoV-2 infection. *Front Cell Neurosci* 17:1285836.
- Carossino M, et al. (2022) Fatal neurodissemination and SARS-CoV-2 tropism in K18-hACE2 mice is only partially dependent on hACE2 expression. *Viruses* 14:535.
- Choi S, et al. (2024) A longitudinal molecular and cellular lung atlas of lethal SARS-CoV-2 infection in K18-hACE2 transgenic mice. *EBioMedicine* 99:104932.
- Choi R, Gupta R, Finlay JB, Goldstein BJ (2022) Olfactory dysfunction and COVID-19. *Oper Tech Otolaryngol Head Neck Surg* 33:141–146.
- Cooper KW, et al. (2020) COVID-19 and the chemical senses: supporting players take center stage. *Neuron* 107:219–233.
- Dedoni S, Avdoshina V, Camoglio C, Siddi C, Fratta W, Scherma M, Fadda P (2022) K18- and CAG-hACE2 transgenic mouse models and SARS-CoV-2: implications for neurodegeneration research. *Molecules* 27:4142.
- de Melo GD, et al. (2021) COVID-19-related anosmia is associated with viral persistence and inflammation in human olfactory epithelium and brain infection in hamsters. *Sci Transl Med* 13:eabf8396.
- Dey R, Bishayi B (2023) Microglial inflammatory responses to SARS-CoV-2 infection: a comprehensive review. *Cell Mol Neurobiol* 44:2.
- Domingues RB, et al. (2020) First case of SARS-COV-2 sequencing in cerebrospinal fluid of a patient with suspected demyelinating disease. *J Neurol* 267:3154–3156.
- Dong W, et al. (2022) The K18-human ACE2 transgenic mouse model recapitulates non-severe and severe COVID-19 in response to an infectious dose of the SARS-CoV-2 virus. *J Virol* 96:e0096421.
- Dusedau HP, et al. (2021) Influenza A virus (H1N1) infection induces microglial activation and temporal dysbalance in glutamatergic synaptic transmission. *mBio* 12:e0177621.
- Eberhardt N, et al. (2023) SARS-CoV-2 infection triggers pro-atherogenic inflammatory responses in human coronary vessels. *Nat Cardiovasc Res* 2:899–916.
- Esposito F, Cirillo M, De Micco R, Caiazzo G, Siciliano M, Russo AG, Monari C, Coppola N, Tedeschi G, Tessitore A (2022) Olfactory loss and brain connectivity after COVID-19. *Hum Brain Mapp* 43:1548–1560.
- Esposito F, Cirillo M, De Micco R, Caiazzo G, Siciliano M, Russo AG, Monari C, Coppola N, Tedeschi G, Tessitore A (2023) Olfactory loss and brain connectivity after COVID-19: structural follow-up at one year. *Neural Plast* 2023:6496539.
- Farbman AI, Margolis FL (1980) Olfactory marker protein during ontogeny: immunohistochemical localization. *Dev Biol* 74:205–215.
- Fernandez-Castaneda A, et al. (2022) Mild respiratory COVID can cause multi-lineage neural cell and myelin dysregulation. *Cell* 185:2452–2468.e16.
- Finlay JB, et al. (2022) Persistent post-COVID-19 smell loss is associated with immune cell infiltration and altered gene expression in olfactory epithelium. *Sci Transl Med* 14:eadd0484.
- Fodoulian L, et al. (2020) SARS-CoV-2 receptors and entry genes are expressed in the human olfactory neuroepithelium and brain. *iScience* 23:101839.
- Frere JJ, et al. (2022) SARS-CoV-2 infection in hamsters and humans results in lasting and unique systemic perturbations after recovery. *Sci Transl Med* 14:eabq3059.
- Garg RK, Paliwal VK, Gupta A (2021) Encephalopathy in patients with COVID-19: a review. *J Med Virol* 93:206–222.
- Golden JW, et al. (2020) Human angiotensin-converting enzyme 2 transgenic mice infected with SARS-CoV-2 develop severe and fatal respiratory disease. *JCI Insight* 5:e142032.
- Golden JW, et al. (2022) Hamsters expressing human angiotensin-converting enzyme 2 develop severe disease following exposure to SARS-CoV-2. *mBio* 13:e0290621.
- Guo Z, Packard A, Krolewski RC, Harris MT, Manglapus GL, Schwob JE (2010) Expression of pax6 and sox2 in adult olfactory epithelium. *J Comp Neurol* 518:4395–4418.
- Harkema JR, Carey SA, Wagner JG (2006) The nose revisited: a brief review of the comparative structure, function, and toxicologic pathology of the nasal epithelium. *Toxicol Pathol* 34:252–269.
- Hoogland IC, Houbolt C, van Westerloo DJ, van Gool WA, van de Beek D (2015) Systemic inflammation and microglial activation: systematic review of animal experiments. *J Neuroinflammation* 12:114.
- Huang C, et al. (2020) Clinical features of patients infected with 2019 novel coronavirus in Wuhan, China. *Lancet* 395:497–506.
- Iadecola C, Anrather J, Kamel H (2020) Effects of COVID-19 on the nervous system. *Cell* 183:16–27.e11.
- Jeong GU, et al. (2022) SARS-CoV-2 infection of microglia elicits proinflammatory activation and apoptotic cell death. *Microbiol Spectr* 10:e0109122.
- Kaufer C, et al. (2022) Microgliosis and neuronal proteinopathy in brain persist beyond viral clearance in SARS-CoV-2 hamster model. *EBioMedicine* 79:103999.
- Khan M, et al. (2021) Visualizing in deceased COVID-19 patients how SARS-CoV-2 attacks the respiratory and olfactory mucosae but spares the olfactory bulb. *Cell* 184:5932–5949.e15.
- Khan M, et al. (2022) Anatomical barriers against SARS-CoV-2 neuroinvasion at vulnerable interfaces visualized in deceased COVID-19 patients. *Neuron* 110:3919–3935.e16.
- Kishimoto-Urata M, et al. (2022) Prolonged and extended impacts of SARS-CoV-2 on the olfactory neurocircuit. *Sci Rep* 12:5728.
- Krasemann S, et al. (2017) The TREM2-APOE pathway drives the transcriptional phenotype of dysfunctional microglia in neurodegenerative diseases. *Immunity* 47:566–581.e9.
- Kumari P, Rothan HA, Natekar JP, Stone S, Pathak H, Strate PG, Arora K, Brinton MA, Kumar M (2021) Neuroinvasion and encephalitis following intranasal inoculation of SARS-CoV-2 in K18-hACE2 mice. *Viruses* 13:132.
- Lamers MM, Haagmans BL (2022) SARS-CoV-2 pathogenesis. *Nat Rev Microbiol* 20:270–284.
- Lappe-Siefke C, Goebbels S, Gravel M, Nicksch E, Lee J, Braun PE, Griffiths IR, Nave KA (2003) Disruption of Cnp1 uncouples oligodendroglial functions in axonal support and myelination. *Nat Genet* 33:366–374.
- Lechien JR, et al. (2020) Olfactory and gustatory dysfunctions as a clinical presentation of mild-to-moderate forms of the coronavirus disease (COVID-19): a multicenter European study. *Eur Arch Otorhinolaryngol* 277:2251–2261.
- Lee IT, et al. (2020) ACE2 localizes to the respiratory cilia and is not increased by ACE inhibitors or ARBs. *Nat Commun* 11:5453.
- Li YC, Bai WZ, Hashikawa T (2020) The neuroinvasive potential of SARS-CoV2 may play a role in the respiratory failure of COVID-19 patients. *J Med Virol* 92:552–555.
- Lier J, Streit WJ, Bechmann I (2021) Beyond activation: characterizing microglial functional phenotypes. *Cells* 10:2236.
- Luczo JM, Edwards SJ, Ardipradja K, Suen WW, Au GG, Marsh GA, Godde N, Rootes CL, Bingham J, Sundaramoorthy V (2024) SARS-CoV and SARS-CoV-2 display limited neuronal infection and lack the ability to transmit within synaptically connected axons in stem cell-derived human neurons. *J Neurovirol* 30:39–51.
- Lyou KS, et al. (2022) Direct neuronal infection of SARS-CoV-2 reveals cellular and molecular pathology of chemosensory impairment of COVID-19 patients. *Emerg Microbes Infect* 11:406–411.
- Mao L, et al. (2020) Neurologic manifestations of hospitalized patients with coronavirus disease 2019 in Wuhan, China. *JAMA Neurol* 77:683–690.
- Mao T, et al. (2022) Unadjuvanted intranasal spike vaccine elicits protective mucosal immunity against sarbecoviruses. *Science* 378:eabo2523.
- Martin-Lopez E, Blanchart A, De Carlos JA, Lopez-Mascaraque L (2011) Dab1 (Disable homolog-1) reelin adaptor protein is overexpressed in the olfactory bulb at early postnatal stages. *PLoS One* 6:e26673.
- Martin-Lopez E, Ishiguro K, Greer CA (2019a) The laminar organization of piriform cortex follows a selective developmental and migratory program established by cell lineage. *Cereb Cortex* 29:1–16.

- Martin-Lopez E, Xu C, Liberia T, Meller SJ, Greer CA (2019b) Embryonic and postnatal development of mouse olfactory tubercle. *Mol Cell Neurosci* 98:82–96.
- Matschke J, et al. (2020) Neuropathology of patients with COVID-19 in Germany: a post-mortem case series. *Lancet Neurol* 19:919–929.
- Maurya DK, Henriques T, Marini M, Pedemonte N, Galletta LJ, Rock JR, Harfe BD, Menini A (2015) Development of the olfactory epithelium and nasal glands in TMEM16A^{-/-} and TMEM16A^{+/+} mice. *PLoS One* 10:e0129171.
- McCray PB Jr, et al. (2007) Lethal infection of K18-hACE2 mice infected with severe acute respiratory syndrome coronavirus. *J Virol* 81:813–821.
- McWhorter FY, Wang T, Nguyen P, Chung T, Liu WF (2013) Modulation of macrophage phenotype by cell shape. *Proc Natl Acad Sci U S A* 110:17253–17258.
- Meinhardt J, et al. (2021) Olfactory transmucosal SARS-CoV-2 invasion as a port of central nervous system entry in individuals with COVID-19. *Nat Neurosci* 24:168–175.
- Meinhardt J, Streit S, Dittmayer C, Manitus RV, Radbruch H, Heppner FL (2024) The neurobiology of SARS-CoV-2 infection. *Nat Rev Neurosci* 25:30–42.
- Meller SJ, Hernandez L, Martin-Lopez E, Kloos ZA, Liberia T, Greer CA (2023) Microglia maintain homeostatic conditions in the developing rostral migratory stream. *eNeuro* 10:ENEURO.0197-22.2023.
- Merad M, Blish CA, Sallusto F, Iwasaki A (2022) The immunology and immunopathology of COVID-19. *Science* 375:1122–1127.
- Monje M, Iwasaki A (2022) The neurobiology of long COVID. *Neuron* 110:3484–3496.
- Moriguchi T, et al. (2020) A first case of meningitis/encephalitis associated with SARS-coronavirus-2. *Int J Infect Dis* 94:55–58.
- Neville KR, Haberly LB (2004) Olfactory cortex. In: *The synaptic organization of the brain*, Ed 5 (Shepherd GM, ed), pp 67. USA: Oxford University Press.
- Oladunni FS, et al. (2020) Lethality of SARS-CoV-2 infection in K18 human angiotensin-converting enzyme 2 transgenic mice. *Nat Commun* 11:6122.
- Olivarria GM, et al. (2022) Microglia do not restrict SARS-CoV-2 replication following infection of the central nervous system of K18-human ACE2 transgenic mice. *J Virol* 96:e0196921.
- Paniz-Mondolfi A, Bryce C, Grimes Z, Gordon RE, Reidy J, Lednický J, Sordillo EM, Fowkes M (2020) Central nervous system involvement by severe acute respiratory syndrome coronavirus-2 (SARS-CoV-2). *J Med Virol* 92:699–702.
- Pellegrini L, Albecka A, Mallery DL, Kellner MJ, Paul D, Carter AP, James LC, Lancaster MA (2020) SARS-CoV-2 infects the brain choroid plexus and disrupts the blood-CSF barrier in human brain organoids. *Cell Stem Cell* 27:951–961.e5.
- Poloni TE, et al. (2021) COVID-19-related neuropathology and microglial activation in elderly with and without dementia. *Brain Pathol* 31:e12997.
- Priyal, Sehgal V, Kapila S, Taneja R, Mehmi P, Gulati N (2023) Review of neurological manifestations of SARS-CoV-2. *Cureus* 15:e38194.
- Ramani A, et al. (2020) SARS-CoV-2 targets neurons of 3D human brain organoids. *EMBO J* 39:e106230.
- Savelieff MG, Feldman EL, Stino AM (2022) Neurological sequelae and disruption of neuron-glia homeostasis in SARS-CoV-2 infection. *Neurobiol Dis* 168:105715.
- Seehusen F, et al. (2022) Neuroinvasion and neurotropism by SARS-CoV-2 variants in the K18-hACE2 mouse. *Viruses* 14:1020.
- Shepherd GM, Rowe TB, Greer CA (2021) An evolutionary microcircuit approach to the neural basis of high dimensional sensory processing in olfaction. *Front Cell Neurosci* 15:658480.
- Shimizu S, et al. (2024) SARS-CoV-2 induces inflammation and intracranial infection through the olfactory epithelium-olfactory bulb pathway in non-human primates. *J Neuroimmunol* 387:578288.
- Sia SF, et al. (2020) Pathogenesis and transmission of SARS-CoV-2 in golden hamsters. *Nature* 583:834–838.
- Soltys Z, Ziąja M, Pawlinski R, Setkowicz Z, Janeczko K (2001) Morphology of reactive microglia in the injured cerebral cortex. Fractal analysis and complementary quantitative methods. *J Neurosci Res* 63:90–97.
- Song E, et al. (2021) Neuroinvasion of SARS-CoV-2 in human and mouse brain. *J Exp Med* 218:e20202135.
- Stein SR, et al. (2022) SARS-CoV-2 infection and persistence in the human body and brain at autopsy. *Nature* 612:758–763.
- Torabi A, et al. (2020) Proinflammatory cytokines in the olfactory mucosa result in COVID-19 induced anosmia. *ACS Chem Neurosci* 11:1909–1913.
- Tsukahara T, Brann DH, Datta SR (2023) Mechanisms of SARS-CoV-2-associated anosmia. *Physiol Rev* 103:2759–2766.
- Ueha R, Ito T, Furukawa R, Kitabatake M, Oujii-Sageshima N, Ueha S, Koyama M, Uranaka T, Kondo K, Yamasoba T (2022) Oral SARS-CoV-2 inoculation causes nasal viral infection leading to olfactory bulb infection: an experimental study. *Front Cell Infect Microbiol* 12:924725.
- Ueha R, Kondo K, Kagoya R, Shichino S, Shichino S, Yamasoba T (2021) ACE2, TMPRSS2, and Furin expression in the nose and olfactory bulb in mice and humans. *Rhinology* 59:105–109.
- Urata S, Maruyama J, Kishimoto-Urata M, Sattler RA, Cook R, Lin N, Yamasoba T, Makishima T, Paessler S (2021) Regeneration profiles of olfactory epithelium after SARS-CoV-2 infection in golden Syrian hamsters. *ACS Chem Neurosci* 12:589–595.
- Varatharaj A, et al. (2020) Neurological and neuropsychiatric complications of COVID-19 in 153 patients: a UK-wide surveillance study. *Lancet Psychiatry* 7:875–882.
- Vassar R, Ngai J, Axel R (1993) Spatial segregation of odorant receptor expression in the mammalian olfactory epithelium. *Cell* 74:309–318.
- Verma AK, Zheng J, Meyerholz DK, Perlman S (2022) SARS-CoV-2 infection of sustentacular cells disrupts olfactory signaling pathways. *JCI Insight* 7:e160277.
- Vidal E, et al. (2022) Chronological brain lesions after SARS-CoV-2 infection in hACE2-transgenic mice. *Vet Pathol* 59:613–626.
- Villadiego J, et al. (2023) Full protection from SARS-CoV-2 brain infection and damage in susceptible transgenic mice conferred by MVA-CoV2-S vaccine candidate. *Nat Neurosci* 26:226–238.
- Wesson DW (2020) The tubular striatum. *J Neurosci* 40:7379–7386.
- Yang L, et al. (2024) SARS-CoV-2 infection causes dopaminergic neuron senescence. *Cell Stem Cell* 31:196–211.e6.
- Ye Q, et al. (2021) SARS-CoV-2 infection in the mouse olfactory system. *Cell Discov* 7:49.
- Yinda CK, et al. (2021) K18-hACE2 mice develop respiratory disease resembling severe COVID-19. *PLoS Pathog* 17:e1009195.
- Yu P, Deng W, Bao L, Qu Y, Xu Y, Zhao W, Han Y, Qin C (2022) Comparative pathology of the nasal epithelium in K18-hACE2 Tg mice, hACE2 Tg mice, and hamsters infected with SARS-CoV-2. *Vet Pathol* 59:602–612.
- Zabel MK, Kirsch WM (2013) From development to dysfunction: microglia and the complement cascade in CNS homeostasis. *Ageing Res Rev* 12:749–756.
- Zapiec B, Mombaerts P (2020) The zonal organization of odorant receptor gene choice in the main olfactory epithelium of the mouse. *Cell Rep* 30:4220–4234.e25.
- Zazhytska M, et al. (2022) Non-cell-autonomous disruption of nuclear architecture as a potential cause of COVID-19-induced anosmia. *Cell* 185:1052–1064.e12.
- Zhao X, Gao F (2024) Novel omicron variants enhance anchored recognition of TMEM106B: a new pathway for SARS-CoV-2 cellular invasion. *J Phys Chem Lett* 15:671–680.
- Zheng J, et al. (2021) COVID-19 treatments and pathogenesis including anosmia in K18-hACE2 mice. *Nature* 589:603–607.
- Ziuzia-Januszewska L, Januszewski M (2022) Pathogenesis of olfactory disorders in COVID-19. *Brain Sci* 12:449.